N. KRISHNAMURTHY
JULY 1971

Preprints

of the

First International Conference on

STRUCTURAL MECHANICS IN REACTOR TECHNOLOGY

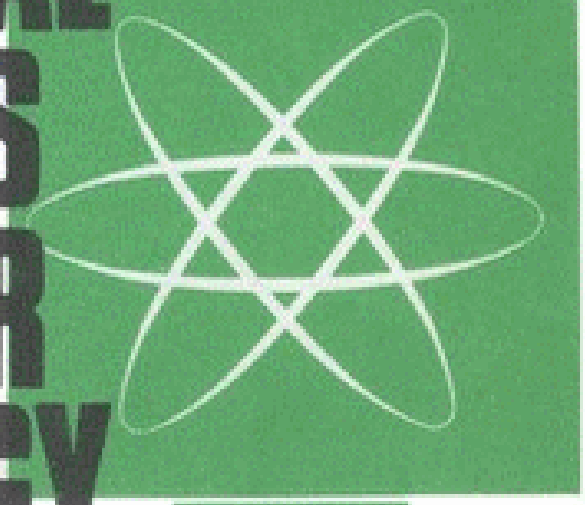

Berlin, Germany · 20 - 24 September 1971

Vol. 3 REACTOR PRESSURE VESSELS

Part G. Steel Pressure Vessels

compiled by: Thomas A. Jaeger

Organized by:

Bundesanstalt für Materialprüfung (BAM), Berlin

Commission of the European Communities, Brussels

in cooperation with: FIRL IKT IPPT ISD NIS NUS SDK

THREE-DIMENSIONAL FINITE ELEMENT ANALYSIS OF THICK-WALLED PIPE-NOZZLE JUNCTIONS WITH CURVED TRANSITIONS

N. KRISHNAMURTHY,

School of Engineering and Engineering Experiment Station, Auburn University, Auburn, Alabama, U.S.A.

ABSTRACT

The stress distribution at the junctions of thick-walled pressure vessels and pipes is of considerable theoretical and practical importance in nuclear reactor technology. This paper reports the three-dimensional finite element idealization and analysis of a typical cylindrical-vessel-nozzle junction. Mathematical relationships are developed defining the geometry of the surface and interior points of thick-walled vessel-nozzle junctions with curved transitions. The computer program developed for the automatic generation of cylindrical coordinates for the three-dimensional idealization of the junction, is briefly described. The principal features of the finite element computer program used for the three-dimensional stress analysis, are presented. The application of the programs to idealize and analyze a typical vessel-nozzle junction for three mesh sizes is outlined, and the results are discussed. A stress concentration factor is evaluated for the problem studied. The study demonstrates the feasibility of three-dimensional finite element idealization and analysis of heavy-section vessel-nozzle junctions, and the general applicability to further investigations. The results indicate a region of high stress concentration in the transition region on the inner surface of the junction, at the longitudinal section.

1. INTRODUCTION

An urgent need exists for a clear understanding of the stress distribution in thick-walled pressure vessels and pipes, at the regions where they connect with nozzles and branches. The bulk of the information available is the result of analytical and experimental investigations on thin-walled sections. Thick-walled sections have been approximately analyzed on the basis of such simplifying assumptions as the applicability of shell theory. However, the validity of these methods and their results will be doubtful, particularly at the transition region where stress concentrations are known to exist. A realistic examination of thick sections requires a three-dimensional analysis.

Due to the complex configuration of the typical vessel-nozzle junction, classical mathematical methods of stress analysis are not conveniently applicable. Finite element methods are the logical choice for such a situation. However, three-dimensional finite element analyses present certain complexities of their own, both in the idealization and in the computational processes, and have not been as widely applied as the two-dimensional programs. Thus, very little information appears to exist on the three-dimensional stress analysis of thick-walled pressure vessel connections.

As part of the simulated service activity of the Heavy Section Steel Technology (HSST) Program at the Oak Ridge National Laboratory (ORNL), operated by the Union Carbide Corporation for the United States Atomic Energy Commission (USAEC), the study was undertaken, to examine by three-dimensional finite element techniques, the stress distribution due to internal pressure, in a typical vessel-nozzle junction with the form and dimensions shown in Fig. 1. Complete details of the study are given in the author's report to the USAEC, [1].

2. FINITE ELEMENT IDEALIZATION OF JUNCTION

2.1. Preliminary Considerations

The study was limited to the particular vessel-nozzle configuration pictured in Fig. 2, and defined by the following considerations:

(1) The vessel and the nozzle are both cylindrical, with straight axes intersecting at right angles. Thus the nozzle is radially attached to the vessel.

(2) The radius and the wall thickness of both the vessel and the nozzle are constant over the portion of the junction analyzed.

(3) Both the inner and outer transitions between the vessel and the nozzle are circular arcs, but not necessarily concentric.

(4) Each transition arc connects tangentially with both the vessel and the nozzle.

For the proposed investigation of stress distribution in and near the nozzle attachment region, the cylindrical coordinate system indicated in Fig. 2 was considered appropriate, with the z-axis along the nozzle axis. The intersection of the axes of the vessel and the nozzle was chosen as the origin.

In conformity with accepted terminology, planes containing the nozzle (z-) axis are referred to as "meridional planes," and planes normal to the nozzle axis as "latitudinal planes." The meridional plane such as QPST in Fig. 2, containing the vessel axis, is the "longitudinal plane," and will be used as the reference plane $\theta = 0$. The meridional plane such as QRV, normal to the vessel axis, is the "transverse plane," and has a value of 90 degrees for θ in the right-handed system used. The latitudinal plane TUV through the origin

is the "equatorial plane." Distances and stresses along the r, θ, and z directions are referred to as the "radial," "circumferential," and "axial" distances and stresses.

For internal pressure, symmetry of the vessel-nozzle junction about the longitudinal and transverse planes would have permitted the analysis of one-fourth of the junction, namely the portion QPSXYVR in Fig. 2. However, for simplicity and to take full advantage of a fine mesh in the finite element analysis, symmetry about the equatorial plane was additionally assumed, enabling the analysis of only one-eighth of the junction, namely the portion QPSTUVR. The implications of this assumption will be discussed later. This octant, chosen for the analysis, will be referred to as the "symmetry octant."

Because of the general applicability of the study, the terms "vessel" and "pipe" are used interchangeably. A surface which extends throughout the wall of the pipe-nozzle junction, in a manner similar to its inner and outer surfaces, is referred to as a "layer." The wall of the junction is divided by layers into "slices." The additional special nomenclature used in the discussion is presented in the view of a typical layer, Fig. 3.

The line such as B'B" in Fig. 3, along which the surfaces of the nozzle and the transition meet tangentially, is the "nozzle tangency line" for the layer. Similarly, the line such as C'C", along which the surfaces of the transition and the pipe meet tangentially, is the "pipe tangency line" for the layer. The two tangency lines form the natural topological boundaries between the three regions of the junction, namely the nozzle, the transition, and the pipe. A line such as ABCD in Fig. 3, which is the intersection of a meridional plane with a layer, is a "meridional trace." Meridional traces divide the 90-degree octant into "layer strips." Divisions such as 1-2, 2-3, . . . , on a layer trace, are "trace divisions." The points 1, 2, . . . , on the meridional trace become the "nodes" for the finite element mesh.

2.2. Location of the Tangency Lines

Figure 4 shows a plan view of the portion of the junction chosen for analysis, and an enlarged meridional section for a general angle θ. As can be seen from Figs. 3 and 4, the meridional trace at any value of θ consists of the straight nozzle region AB, the circular arc BC of the transition, and an elliptical curve CD for the pipe region. In Fig. 4, the ellipse quadrant FCDE, of which CD forms a part, has the semi-major axis OE ($=R_p/\sin\theta$), and the semi-minor axis OF ($=R_p$). The equation of the ellipse may therefore be written,

$$r^2 \sin^2\theta + z^2 = R_p^2 \quad , \tag{1}$$

where r and z are the coordinates of any point on the ellipse, and R_p the radius of the pipe layer. (When r and z are subscripted, the subscripts will refer to a particular point.)

When θ is less than θ_ℓ, the angle to the layer corner U, the coordinates of D are given by,

$$r_D = P_\ell/\cos\theta \quad , \tag{2a}$$

and, by substitution into eq. (1),

$$z_D = (R_p^2 - P_\ell^2 \tan^2\theta)^{1/2} \quad , \tag{2b}$$

where P_ℓ is the half-length of pipe chosen for analysis.

When θ is more than θ_ℓ, the coordinates of D' of Fig. 4(a) or Fig. 3 are given by,

$$r_{D'} = R_p/\sin\theta \text{ , and } z_{D'} = 0 \ . \tag{3}$$

To locate the pipe tangency point C on the meridional trace, it may be noted from

Fig. 4(b) that,

$$R_n + R_t = r_G = r_C + R_t \sin \beta \quad , \tag{4}$$

where, R_n and R_t are the radii of the nozzle and transition in the layer, G is the center of curvature of the transition arc, and β is the angle between the radius GC and the z-direction, as also the angle between the tangent at C and the equatorial plane.

Equation (4) gives the expression for sin β as,

$$\sin \beta = (R_n + R_t - r_C)/R_t \quad . \tag{5}$$

Further, from eq. (1) for the ellipse, the expression for the slope of the tangent may be written as,

$$\tan \beta = \left.\frac{dz}{dr}\right|_{r=r_C} = \frac{-r_C \sin^2\theta}{(R_p^2 - r_C^2 \sin^2\theta)^{1/2}} \quad , \tag{6}$$

which, with the sign ignored as not pertinent to the analysis, yields the expression,

$$\sin \beta = \frac{r_C \sin^2\theta}{[R_p^2 - r_C^2(\sin^2\theta \cos^2\theta)]^{1/2}} \quad . \tag{7}$$

When the two values of sin β given by eq. (5) and eq. (7) are equated, the equation for the unknown r_C is obtained as,

$$Ar_C^4 + Br_C^3 + Cr_C^2 + Dr_C + E = 0 \quad , \tag{8a}$$

where, $A = -\sin^2\theta \cos^2\theta$, $B = -2A(R_n + R_t)$,

$C = A(R_n + R_t)^2 + R_p^2 - R_t^2 \sin^4\theta$, $D = 2R_p^2(R_n + R_t)$,

and, $E = R_p^2(R_n + R_t)^2$.

Equation (8a) may be conveniently solved for r_C by the Newton-Raphson method to the desired precision. With r_C known, the z-coordinate of C may be obtained from eq. (1) as,

$$z_C = (R_p^2 - r_C^2 \sin^2\theta)^{1/2} \quad . \tag{8b}$$

For the nozzle tangency point B, Fig. 4(b), and eq. (6) indicate,

$$r_B = R_n \quad , \tag{9a}$$

and,

$$z_B = z_C + R_t \cos \beta = z_C[2R_t(r_C - R_n) - (r_C - R_n)^2]^{1/2} \quad . \tag{9b}$$

2.3. Location of Nodes on Meridional Trace

By dividing the nozzle, transition, and pipe regions into L, M, and N parts in a suitable manner, (L + M + N + 1) nodes may be located on a meridional trace. In this study, the nozzle height AB was divided into L parts. But, to obtain better control over the curved trace divisions, the transition and pipe regions were divided angularly rather than on their projected lengths. The angle BGC subtended by the transition was divided into M parts; the angle COD subtended by the pipe region at the origin was divided into N parts. Figure 4 shows one typical trace division in each of the three regions.

For equal trace divisions in the nozzle region AB, for the node at the end of 'ℓ'th division from A, the coordinates are,

$$r = R_n, \text{ and, } z = z_A - (z_A - z_B)(\ell/L) \quad , \tag{10}$$

where z_A is the maximum height (Z_m) of the nozzle top above the equatorial plane, as chosen for the analysis.

In the transition region BC, the angle BGC subtended by the arc BC is given by,

$$\alpha = \sin^{-1}[(z_B - z_C)/R_t] \quad , \tag{11}$$

and the coordinates for the node at the end of the 'm'th division from B are given by,

$$r = R_n + R_t[1 - \cos(\alpha m/M)] \quad , \tag{12a}$$

and,

$$z = z_B - R_t \sin(\alpha m/M) \quad . \tag{12b}$$

In the pipe region CD, for the node at the end of the 'n'th division from C, the angle γ measured from the equatorial plane is given by,

$$\gamma = \gamma_C - (\gamma_C - \gamma_D)(n/N) \quad , \tag{13}$$

where the values of γ_C and γ_D are given by the expressions $\tan^{-1}(z_C/r_C)$ and $\tan^{-1}(z_D/r_D)$. It must be noted that for a value of θ equal to or larger than θ_ℓ, γ_D will be zero.

If s is the polar distance of the node from the origin O, as marked on Fig. 4, the coordinates of the node are,

$$r = s \cos\gamma, \quad \text{and,} \quad z = s \sin\gamma \ , \tag{14}$$

in which the value of s can be obtained, by substitution for r and z into eq. (1), as,

$$s = R_p/(\sin^2\gamma + \cos^2\gamma \sin^2\theta)^{1/2} \ . \tag{15}$$

By raising to a suitable power, the ratios of the number of intervals upto a node to the total number of nodes in the nozzle or the pipe region, the node spacing may be progressively varied, and in particular nodes may be moved closer to the transition region, for obtaining a smooth gradation of mesh in the region of interest. This exponent will be referred to as the "crowding index."

It may happen that no meridional section passes through the layer corner (U in Fig. 3), in which case, routine element definition procedures may miss the piece UD'9 of the layer. To properly define the slice in the neighborhood of the corner, either an additional element corresponding to the omitted piece must be attached, or one of the two adjacent nodes (D' or 9 in Fig. 3) must be relocated at the corner U. In the study, the latter method was adopted.

2.4. "HST-NODES" Computer Program

A computer program was written, in Fortran IV language, to calculate, by the procedures described in the preceding sections, the nodal coordinates for the finite element mesh of a thick-walled pipe-nozzle junction with curved transition. The computer program is designated "Heavy Section Tee Nodes," and is referred to by the abbreviation "HST-NODES." Complete details, program listing, and input instructions are given in the author's report, [1].

The program is capable of various degrees of automatic mesh generation. When supplied with the inner and outer dimensions of the symmetry octant, the number of slices, angular parts and trace divisions for the idealization, a crowding index and certain options, the program will generate all the additional information necessary for the computations on the intermediate layers, compute the cylindrical coordinates, and print and also punch out on cards in a specified format, the values in sequential order.

Such a completely automatic procedure would develop slices of equal thickness, equal angular divisions, constant crowding index for all θ, and (if L, M, and N are specified the same for the inner and the outer surfaces) constant distribution of the trace divisions in all the layers and for all θ. Greater control over the mesh may be achieved as desired, by specifying the appropriate identifiers, and supplying additional input. Meridional sections may be specified at desired angular locations. Crowding indices may be specified differently

for different meridional sections, and, even on the same meridional section, differently for the nozzle and for the pipe. Nonuniform slices may be obtained by specifying their radii. Trace division distributions may be varied not only from layer to layer, but from one meridional section to another.

Although the program was developed for thick-walled junctions and curved transitions, it has the additional capability to idealize, when appropriate parameters are input, (1) junctions (or layers) with no transition region, that is, sharp junctions, and (2) 'thin-walled' junctions which may be adequately analyzed with two-dimensional (shell) finite element programs.

Further, with a few changes, the program may be modified to idealize a symmetry quadrant (such as the portion QPSXYVR in Fig.2) rather than the octant, thus eliminating the need for assumed symmetry at the equatorial plane. Extensions to the half-pipe and full pipe are then relatively simple, permitting the analysis for unsymmetric loadings and constraints.

3. FINITE ELEMENT ANALYSIS OF THE JUNCTION

During recent years, the basic principles of the displacement method of finite element analysis have become widely known, and large numbers and great variety of complex problems have been solved by the use of many general and special purpose computer programs. In brief, the technique consists in idealizing the continuum into an assemblage of elements connected at the nodes; formulating the equilibrium equations which relate the nodal forces and nodal displacements, on the basis of an assumed displacement field; solving the set of equations, under prescribed boundary constraints and loads, for the unknown displacements; and finally computing the strains and the stresses in the elements. Three-dimensional finite element analysis has not been as extensively applied to solve actual problems, as two-dimensional analyses including plane stress and plane strain, axisymmetric, and plate and shell formulations.

3.1. The "SAFE-3D" Program

The computer program used for the three-dimensional analysis of the pipe-nozzle junction was the "SAFE-3D," the name being the abbreviation for "Stress Analysis by Finite Elements - 3 Dimensional." The program was developed by the General Atomic Division of General Dynamics Corporation, now Gulf General Atomic, Inc., of San Diego, California, U.S.A., under subcontract to the Union Carbide Corporation. It had been originally written for the UNIVAC-1108 computer of General Atomic, and was modified at the Computing Technology Center at Oak Ridge, for use on the IBM System 360.

The program provides a three-dimensional elastic analysis of heterogeneous structures of arbitrary geometry. The basic solid element used in the analysis is the constant strain tetrahedron with (assumed) linear displacement field. In addition to solid regions, any membranes or embedded bars may also be included in the analysis. Problems may be formulated and solved in either the Cartesian or the cylindrical coordinate systems. Analysis for steady-state thermal effects is also possible.

The program capabilities and input instructions for SAFE-3D are given in the User's Manual by Cornell et al., [2]. Although the computational element for the solid regions is the tetrahedron, the input element is the octahedron composed of three tetrahedra, leading to a considerable reduction of input for the element descriptions for the idealized body.

The idealization of the solid continuum into an assemblage of elements is achieved, in effect, by considering the body to be cut into a number of "segments" by means of "sections." The sections, being the bounding surfaces of the solid and the interfaces between the segments,

are defined at (and by) the nodes lying on the surfaces. The segments are subdivided into octahedra by means of transverse planes connecting appropriate nodes from the adjoining sections. Figure 5 illustrates one segment of a solid; a typical octahedral element IJKLMN is shown subdivided into the three component tetrahedra IJKL, JKLM, and KLMN as the program would, internally.

The input procedure for the idealization consists of defining the geometry of the body by the coordinates of the nodes on each section, and describing the topology of the body by the nodal indices of the elements in each segment. The program has an automatic mesh generation feature for regions where the nodes and elements may be described in terms of their initial and final parameters and indices. For such uniform regions, the program interpolates the indices and coordinates of the intermediate nodes, and develops the indices and node definitions of the octahedral elements.

Machine-generated nodes may be "moved" to more preferable locations by reading-in new coordinates. Further input consists of information on: material properties for different groups of elements; loading information for concentrated forces, body forces, surface tractions, and temperature changes; and displacement constraints.

The SAFE-3D program may be run in a number of progressive stages. A full capacity run with the program could involve as many as 5000 nodes; under such conditions, the equilibrium equations would number about 15,000, and the band width of the stiffness matrix would be of the order of 1000. In order to solve equations of such magnitudes, SAFE-3D utilizes a special block iteration technique, described by Rashid, [3]. The precision of the final solution may be controlled by the user, by specifying the number of iterations and the "unbalanced force," namely the tolerable difference between the applied forces and their values recalculated from the displacements of the last iteration. More details of application of the program may be found in the paper by Corum and Krishnamurthy, [4].

3.2. Idealization and Analysis of Junction

The portion of the junction of Fig. 1 selected for the study as the region of interest is shown in Fig. 6. The vessel and the nozzle had internal diameters 27.0 in. and 9.0 in.; the internal and external transition radii were 1.5 in. and 3.0 in. The wall thickness was 6.0 in. for the pipe, and was taken as 6.0 in. for the entire height of the nozzle chosen for the analysis; the configuration shown in Fig. 1 was finalized subsequent to the implementation of the analysis. The maximum height (Z_m) of the nozzle top above the equatorial plane was taken as 40.0 in. Two values of half-pipe lengths (P_ℓ), namely 19.5 in. and 30.0 in. were chosen, to examine any differences in the stress distributions for the two lengths, referred to hereinafter as "short pipe" and "long pipe" cases.

A value of 1000 psi was adopted for the internal pressure, for convenience. The stresses at the "cut" ends of the nozzle and the vessel were assumed uniformly distributed over the cross-sectional areas of the walls, at values which would equilibrate the pressure acting on the areas of the open ends. This condition would correspond to the situation where the nozzle and the vessel were rigidly capped. On this basis, the loading for the symmetry octant consisted of the 1000 psi normal pressure on the internal surface, and uniform tensile stresses of 225.0 psi on the nozzle end and 920.45 psi on the vessel end.

The boundary conditions for the sector were simply the constraints imposed by the symmetry, actual and assumed, namely, zero angular (θ) displacement for the nodes on the longitudinal and transverse sections, and zero axial (z) displacement for the nodes on the

equatorial plane.

Three cases were analyzed, corresponding to three mesh idealizations designated "coarse," "medium," and "fine." Details of the meshes are presented in Table I. Figure 7 depicts the idealization of the symmetry sector for the coarse mesh, complete with the node and element numbering schemes. Figure 8 shows the layout of the fine mesh on the longitudinal and transverse sections. Each mesh was finalized after examining computer plots of the output from HST-NODES for different combinations of L, M, and N, and with various crowding indices.

The node coordinates for each chosen mesh were punched out on cards by the HST-NODES program in a format suitable for the SAFE-3D input deck. An enormous amount of time and effort that would have been normally required for hand input of individual element description cards was saved, and the accompanying risk of error was avoided, by a simple stratagem. The automatic mesh generation routine of the SAFE-3D was utilized to develop the element descriptions for a 90-degree sector of a 'dummy' axisymmetric solid with the same number and general arrangement of nodes and segments as in the octant of the junction. The reading-in of the actual node coordinates for the junction achieved the subsequent modification of the geometry to the desired shape, without affecting the connectivities of the elements.

The analysis of the three cases was carried out in the recommended stages, to precisions corresponding to force imbalances averaging less than 1 lb. per node. Central Processor Unit (CPU) times for the IBM System 360/65 computer used for the analysis were about 25 min., 76 min., and 188 min. for the coarse, medium, and fine meshes.

4. RESULTS OF FINITE ELEMENT ANALYSIS

4.1. Stress Distributions

Examination of the computer output for stresses revealed the following characteristics:

(1) The shear stresses everywhere were generally much smaller than the normal stresses. Further, the regions of high shear stresses and of high normal stresses did not coincide.

(2) The radial stresses σ_r were all within the range of ±1000 psi throughout.

(3) The circumferential stresses σ_θ were maximum on the inner surface at the longitudinal section, near the transition region. The maximum shear stresses in this region were in the latitudinal planes, of magnitude about 5% of the maximum σ_θ values.

(4) The axial stresses σ_z were maximum on the inner surface near the intersection of the transverse section and the equatorial plane. The maximum shear stresses in this region were between 10 and 20% of the maximum axial stresses.

(5) The maximum circumferential stress for any mesh was more than twice the maximum axial stress, and much higher than the maximum radial stress. Further, in the region of maximum σ_θ, the radial and axial stresses were very low, about 15% in magnitude.

On the basis of the preceding observations, it was considered unlikely that the critical principal stresses would be much different from the critical normal stresses themselves. More detailed evaluation was confined to the normal stresses only.

4.2. Stress Contours

The normal stress distributions σ_r, σ_θ, and σ_z were first examined quantitatively by plotting iso-stress lines or "stress contours" on the longitudinal and transverse sections for all three meshes, and on the 45° meridional section additionally for the medium mesh.

The stress variations on meridional sections revealed oscillations analogous to the results from a triangular element discretization of plane stress analysis. An averaging

process was used to smooth out the oscillations, and the average stresses were considered to act at the centroids of the faces of the elements attached to the meridional section.

Contours were interpolated, every 250 psi apart, linearly between adjacent known values, in the interior. Wherever boundary values were known, as applied pressure or end tractions, interpolation was carried right up to the boundary and as far along it as would not violate other computed results.

But where the boundary values were not known, contours were extrapolated up to the boundary at the same gradient as in the adjacent interior interval. This procedure ignored any changes in the stress gradients near a boundary, and it was adopted only as a device to complete the stress plots and thus obtain graphical representations of the general stress distribution over the entire meridional section. More effective extrapolation techniques were used, as will be described later, to predict the maximum values on the boundary.

Figures 9, 10, and 11 show the contour plots of σ_r, σ_θ, and σ_z respectively for all three meshes, on the longitudinal section; Figures 12, 13, and 14 show the corresponding variations on the transverse section. The known boundary values used to plot the contours are indicated on the plots in parentheses. The medium mesh plots for the 45° meridional section (not included herein) indicated a smooth transition between the corresponding plots of the longitudinal and transverse sections.

The effects of the mesh size on the stress distributions may be observed by comparing the plots (a), (b), and (c) for the coarse, medium, and fine meshes, in each of the Figs. 9 to 14. In every case, the stress gradients are seen to change progressively with mesh refinement, the change being generally to increase the gradient, as might be expected. It is also obvious that the critical stress for the case analyzed is the circumferential stress near the inner transition on the longitudinal section.

The effects of the pipe length considered, on the stress distributions, may also be investigated to a limited extent, by comparing the long pipe plot (b) with the short pipe plots (a) and (c) in each of the Figs. 9 to 14. The broken line in the long pipe longitudinal sections (b) of Figs. 9 to 11, drawn at a radial distance of 19.5 in., enables such a comparison with the short pipe domain. It is clearly seen that the patterns of the contours for the short and long pipes are very similar. Further, the medium mesh stress distributions are generally intermediate between the coarse and fine mesh results. Finally, the contours at the 19.5 in. line in the longitudinal section of the medium mesh plots also compare satisfactorily with the corresponding coarse and fine mesh contours at the pipe end. These facts suggest that differences in the lengths of pipe might not significantly affect the stress distribution, especially in the transition region (for lengths larger than about 19.5 in.).

At the equatorial plane where symmetry was assumed contrary to the situation existing in the physical problem, Fig. 14 indicates rather large axial stresses at the transverse section. The maximum contour value of σ_z (2500 psi) is less than 40% of the maximum contour value of σ_θ (6500 psi) in Fig. 10, and the stress gradients are also not as steep. It is therefore further postulated that if the symmetry constraint had not been imposed, the axial stress distribution would have been more uniform at the equatorial plane, and hence even less critical in the analysis than with the assumed symmetry.

4.3. Extrapolation of Surface Stress

The linearly extrapolated values of σ_θ at the inner surface for the coarse, medium, and fine meshes may be estimated from the contour plots Fig. 10 (a), (b), and (c), at 4750, 5500,

and 6500 psi, respectively. To obtain extrapolated values superior to these estimates, it would be necessary to examine the stress variation along a particular line, logically the line of steepest stress gradient.

From Fig. 10, it is apparent that the line of steepest gradient for σ_θ lies in the transition, just below the nozzle region; a convenient line was chosen, as marked EF in Fig. 10(a), joining points on the inner and outer transition arcs where they subtended 15° to the horizontal, at the centers of the respective curves.

For each mesh, the values of σ_θ at points on the critical line EF were determined by interpolation between computed values for elements on or on either side of the line; since such interpolation was done along directions generally normal to the line of steepest gradient, any interpolation error was considered insignificant. The computed values of σ_θ are shown as points in Fig. 15.

Since plots of $(\log \sigma_\theta)$ versus x were nearly straight lines, the expression for the circumferential stress variation along the critical line was assumed in the form,

$$\sigma_\theta = a\, e^{bx} \tag{16}$$

A least squares fit was determined mathematically for each mesh, and the following expressions were obtained:

$$\sigma_\theta = 5163.7\, e^{-0.175\, x} \quad \text{for coarse mesh ,} \tag{17a}$$

$$\sigma_\theta = 6298.5\, e^{-0.210\, x} \quad \text{for medium mesh ,} \tag{17b}$$

and,

$$\sigma_\theta = 6556.6\, e^{-0.211\, x} \quad \text{for fine mesh .} \tag{17c}$$

The maximum stress on the inner surface could then be obtained as the value of σ_θ at E, with x equal to zero; the three values are, 5163.7, 6298.5, and 6556.6 psi. The curves of the three fit expressions are also shown in Fig. 15. The deviations of the curves from the computed values are well within computational and algorithmic accuracy, with a maximum difference less than 3.6%.

4.4. Extrapolation to the Continuum

It is obvious from the circumferential stress variations along the critical line, that with further refinement of mesh, the maximum value would rise, and converge asymptotically to the value for the continuum. To predict a value for the continuum from the three available maximum stress values, the stress must be related to the mesh size either in terms of a suitable parameter (h) for element size, or the number (m) of nodes.

Since the mesh size was not constant over the region, the number of nodes in a domain common to all three cases is the preferable basis of comparison. The largest common domain as the one for the short pipe cases of coarse and fine meshes, having 504 and 2112 nodes. Of the 1170 nodes in the long pipe (medium mesh) case, approximately 50 nodes could be assigned to its extra pipe length; thus the equivalent number of nodes for the medium mesh was taken as 1120. This common domain will be referred to as the "short pipe domain." A comparison may also be made on a partial domain, in particular the transition region. This would exclude the widely different size gradations which occur in the same mesh, toward the nozzle and pipe ends. The node count for this "transition domain" gives 112, 198, and 339 nodes for the coarse, medium, and fine meshes, respectively.

Plots of maximum σ_θ against normalized reciprocals of node counts for the two domains are shown in Fig. 16. The number of coarse mesh nodes (m_c) is used for the normalizing and ues plotted for exponents of 1 and 2, to show the variation. The short pipe domain curves

indicate that σ_θ versus $(m_c/m_a)^n$ would yield a straight line for some value of n between 1.0 and 2.0. The transition domain curves suggest that σ_θ versus (m_c/m_b) would be linear for n slightly more than 2.0.

The variation of σ_θ with mesh size may hence be assumed in the form,

$$\sigma_\theta = a + b(m_c/m)^n \quad , \tag{18}$$

and the two sets of available values used to solve for a, b, and n for the two domains. The two expressions thus obtained are,

$$\sigma_\theta = 6694.0 - 1530.0\ (m_c/m_b)^{1.70} \quad \text{for the short pipe domain,} \tag{19a}$$

and,

$$\sigma_\theta = 6644.0 - 1480.0\ (m_c/m_b)^{2.55} \quad \text{for the transition domain.} \tag{19b}$$

The value for the continuum can now be found as the extrapolated value at (1/m) of zero, corresponding to an infinite number of elements of infinitesimal size; the absolute maximum circumferential stress for the continuum thus becomes 6694.0 psi for the short pipe domain, and 6644.0 psi for the transition domain, of which the larger value may be chosen as the more critical. The rounded-off value 6700 psi may thus be adopted as the absolute maximum stress in the continuum.

4.5. Stress Concentration Factor

The normal stress σ' in the pipe-nozzle junction is defined as,

$$\sigma' = p\, R_{pi}/t \quad , \tag{20}$$

where, p is the internal pressure, R_{pi} the internal radius of the pipe, and t the thickness of the pipe wall. In the present study, the nominal stress is obtained as 2250 psi.

Hence the stress concentration factor for the junction, under the loading and boundary conditions analyzed, is,

$$K = \sigma_{\theta(max)}/\sigma' = 6700.0/2250.0 = 2.98 \ .$$

The value may be rounded off to 3.0. The maximum stress is a tension in the circumferential direction, occuring in the transition region on the inner surface, just below the nozzle tangency point on the longitudinal section.

5. CONCLUSION

A massive computational effort went into the analysis, and very voluminous output was evaluated, apparently to arrive at the single number representing the stress concentration factor for a particular case. However, the problem studied was one in which precise analysis was lacking but essential, and hence the present study must first be considered as demonstrating the feasibility of analyzing a complex junction by a completely general three-dimensional analysis based on a realistic and (in the limit) exact algorithm; the qualitative observations may increase the understanding of the basic problem.

Second, while three-dimensional finite element programs and their use are increasing, the discretization of complex solids continues to be a very intricate and tedious task. The technique and the computer program developed in the study may enable the automatic discretization of vessel-nozzle junctions in further investigations.

ACKNOWLEDGEMENT

The study was sponsored by the Heavy Section Steel Technology Program of the USAEC at

ORNL, and was performed by the author under subcontract to Union Carbide Corporation. Appreciation is due F. J. Witt, Director of the HSST Program for his continued support, and J. S. Crowell of the Computing Technology Center for carrying out the computer solutions.

REFERENCES

[1] KRISHNAMURTHY, N., "Three-Dimensional Finite Element Analysis of Thick-Walled Vessel-Nozzle Junctions with Curved Transitions," Heavy Section Steel Technology Program Technical or Programmatic Manuscript No. 11, ORNL-TM-3315, Oak Ridge National Laboratory, Oak Ridge, Tennessee, U.S.A., (1970).

[2] CORNELL, D. C., et al., "SAFE-3D. A Computer Program for the Three-Dimensional Stress Analysis of Composite Structures, A User's Manual," USAEC Report GA-7855, General Atomic Division, General Dynamics Corporation, San Diego, California, U.S.A., (1967).

[3] RASHID, Y. R., "Three-Dimensional Analysis of Elastic Solids," USAEC Report GA-8419, Gulf General Atomic Inc., San Diego, California, U.S.A., (1968).

[4] CORUM, J. M., and KRISHNAMURTHY, N., "A Three-Dimensional Finite Element Analysis of a Prestressed Concrete Reactor Vessel Model," Proceedings of the Symposium on Application of Finite Element Methods in Civil Engineering, pp. 63-94, Vanderbilt University School of Engineering and American Society of Civil Engineers, U.S.A., (1969).

TABLE I

MESH DETAILS FOR THE THREE CASES ANALYZED

Item	Coarse Mesh	Medium Mesh	Fine Mesh
ipe designation and length	Short, 19.5 in.	Long, 30.0 in.	Short, 19.5 in.
umber of slices	3 (equal)	4 (equal)	5 (unequal)
umber of angular divisions	6 (of 15°)	8 (of 11.25°)	10 (of 9°)
, M, N on inner layer*	7, 3, 7	11, 3, 11	(19-17), 3, (9-11)
, M, N on outer layer*	7, 3, 7	11, 4, 10	(15-17), (7-3), (9-11)
Number of trace divisions	17	25	31
ozzle crowding index*	0.60	0.60 to 0.64	0.80
ipe crowding index*	0.60	0.91 to 0.75	0.95 to 0.80
umber of nodes	504	1170	2112
umber of octahedral elements	612	1600	3100

Where the value is given as a range, the two numbers refer to the longitudinal and transverse sections, respectively.

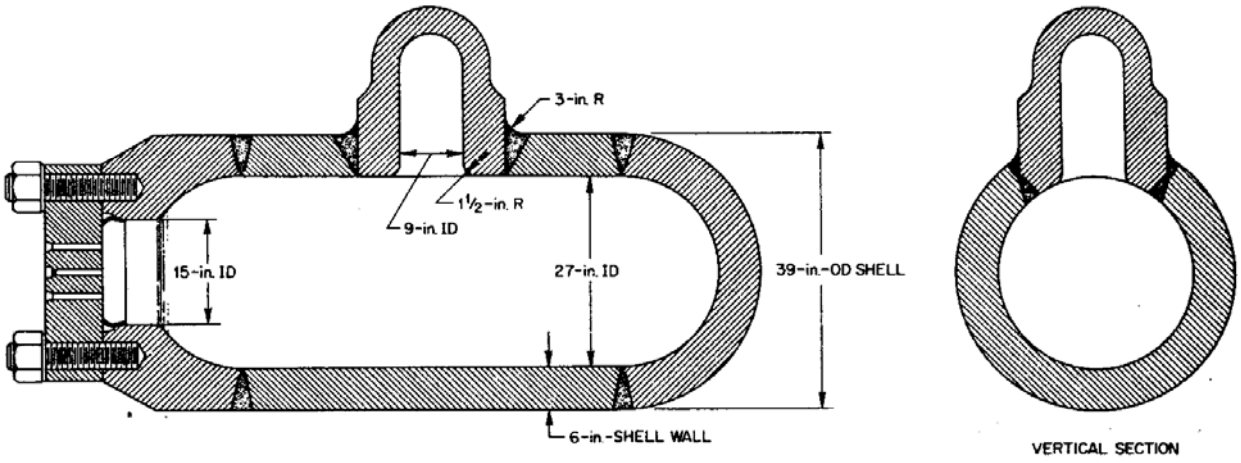

Fig. 1. Intermediate Test Vessel-Nozzle Junction of USAEC-HSST Program.

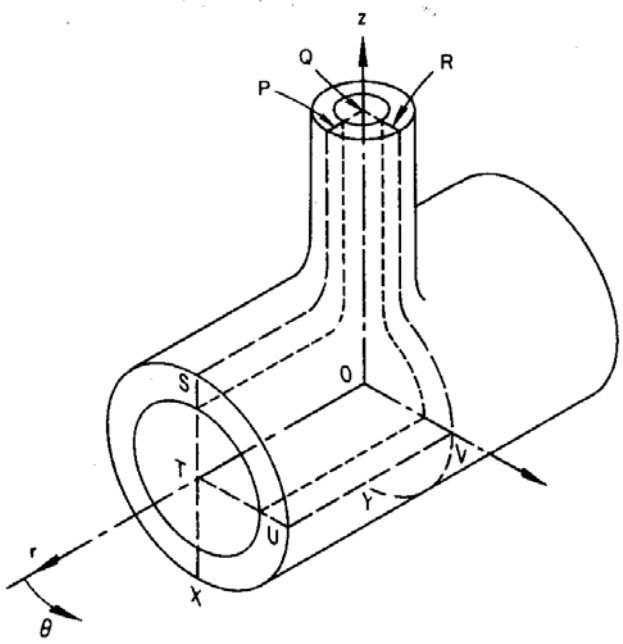

Fig. 2. Configuration of Vessel-Nozzle Junction for Finite Element Analysis.

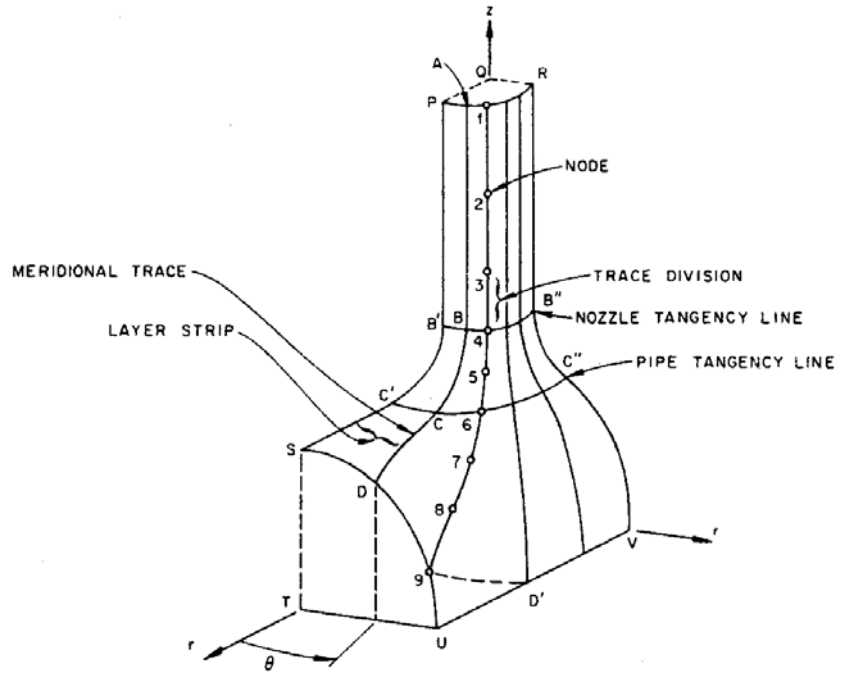

Fig. 3. A Layer from the Symmetry Octant of the Junction.

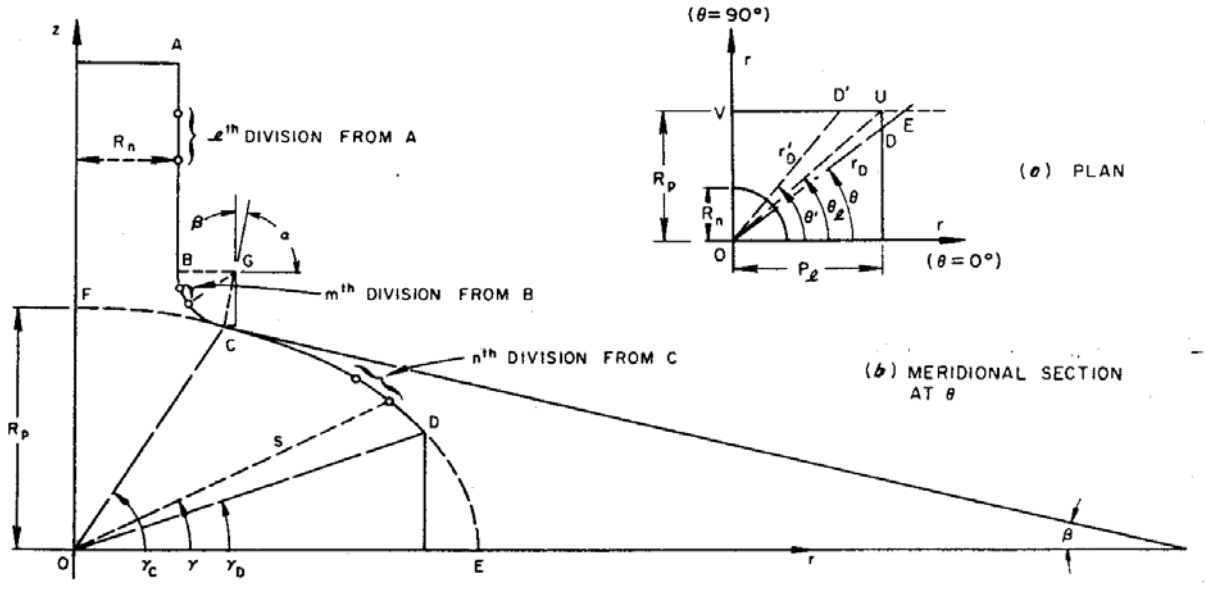

Fig. 4. Plan, and Typical Meridional Trace of a Layer.

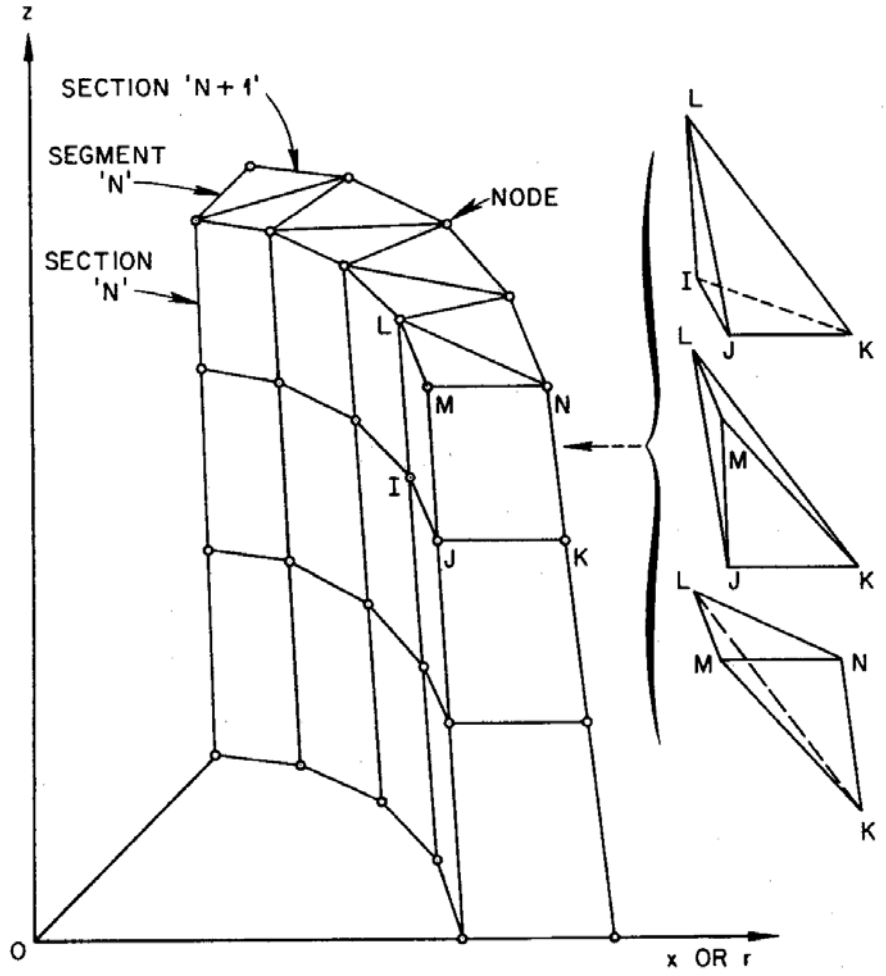

Fig. 5. Segment of a Solid, and Component Tetrahedra of a Typical Octahedron.

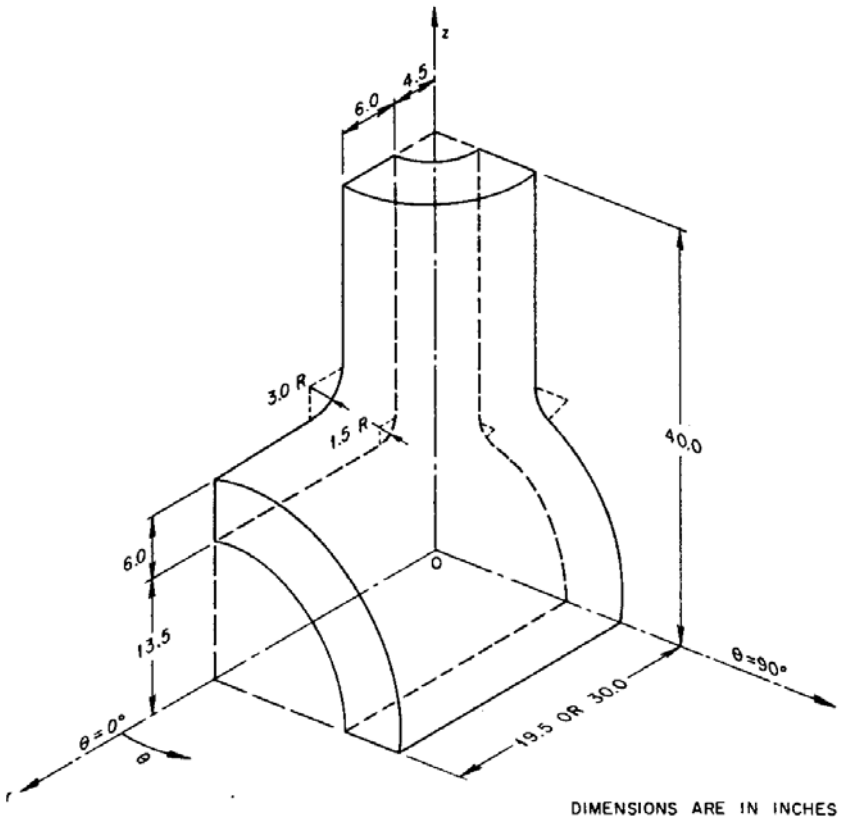

Fig. 6. Dimensions of the Symmetry Octant of Junction Analyzed.

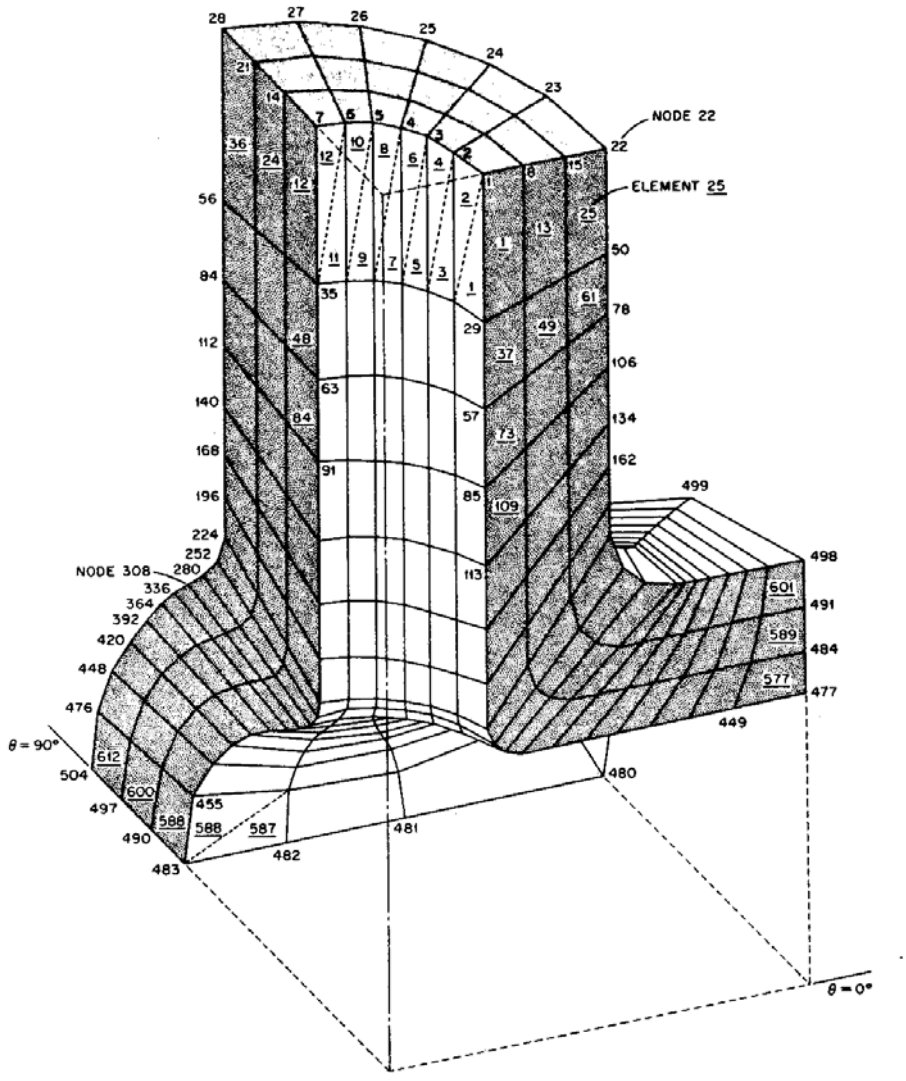

Fig. 7. Coarse Mesh Idealization Scheme. (Element indices underscored.)

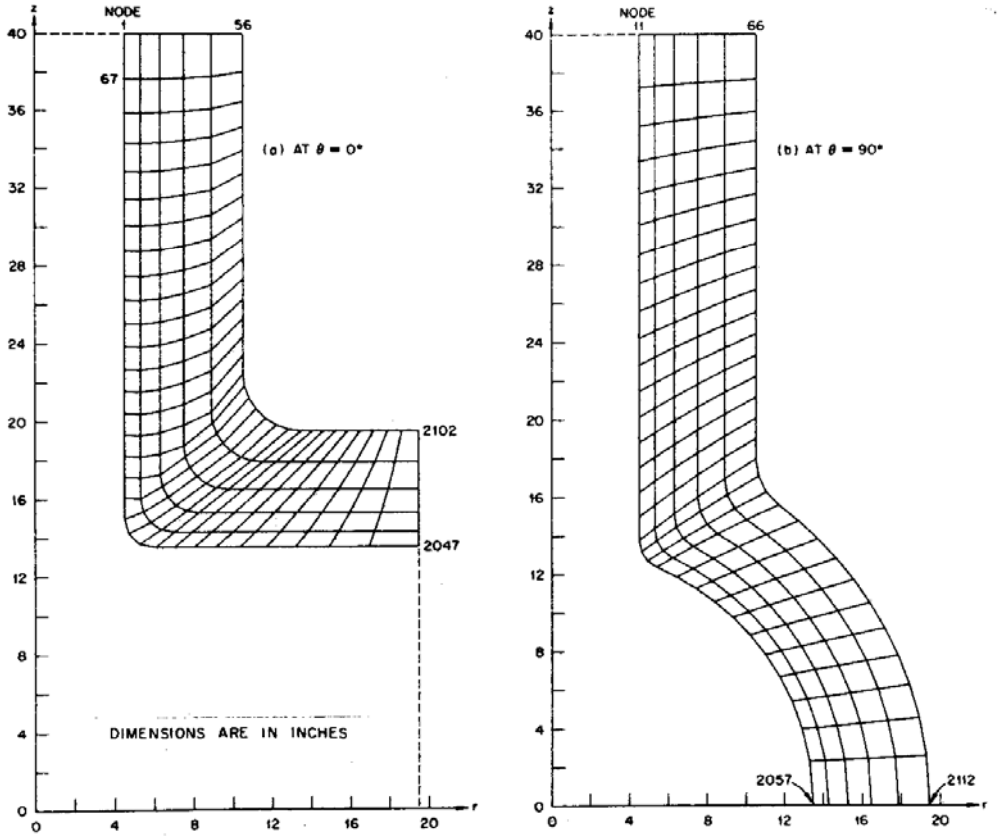

Fig. 8. Fine Mesh Layout at Longitudinal and Transverse Sections.

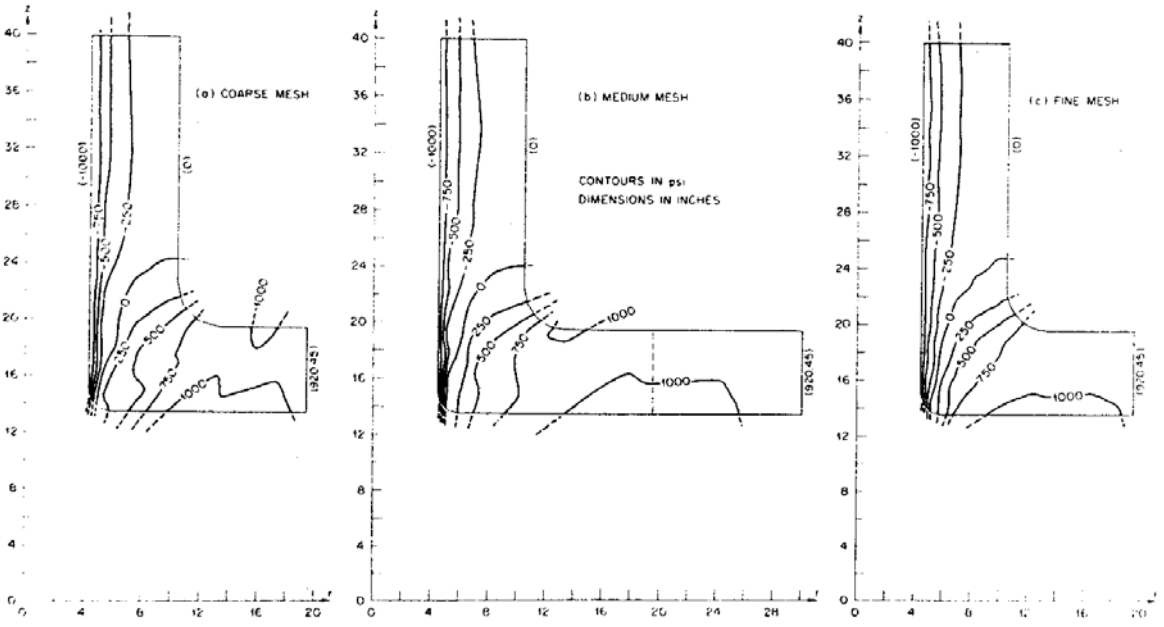

Fig. 9. Radial Stress (σ_r) Contours on Longitudinal Section.

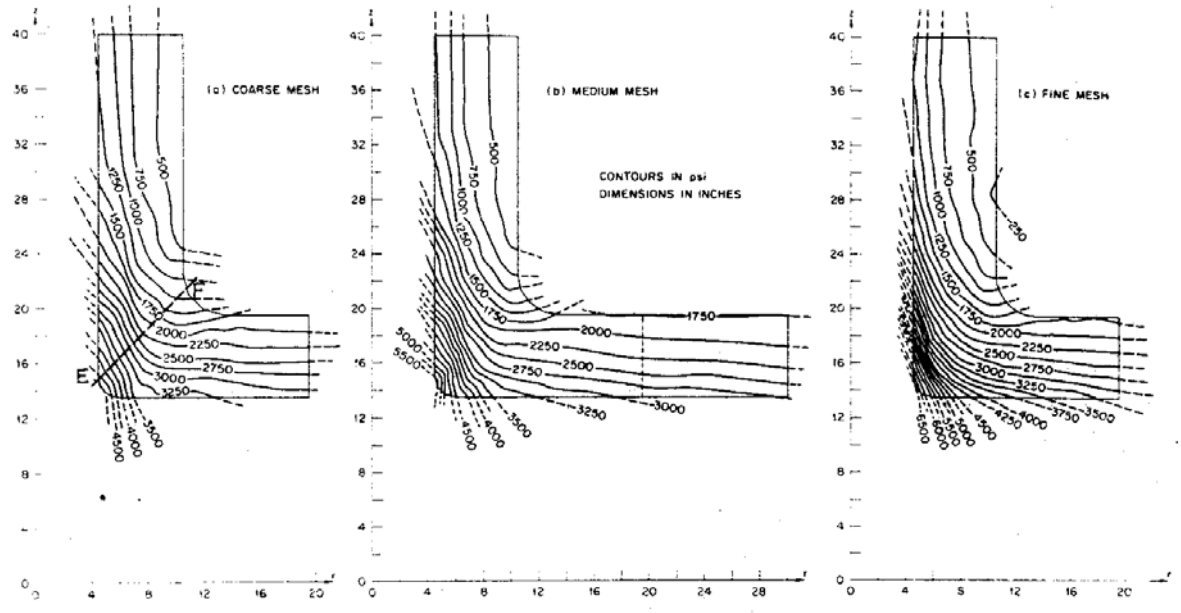

Fig. 10. Circumferential Stress (σ_θ) Contours on Longitudinal Section.

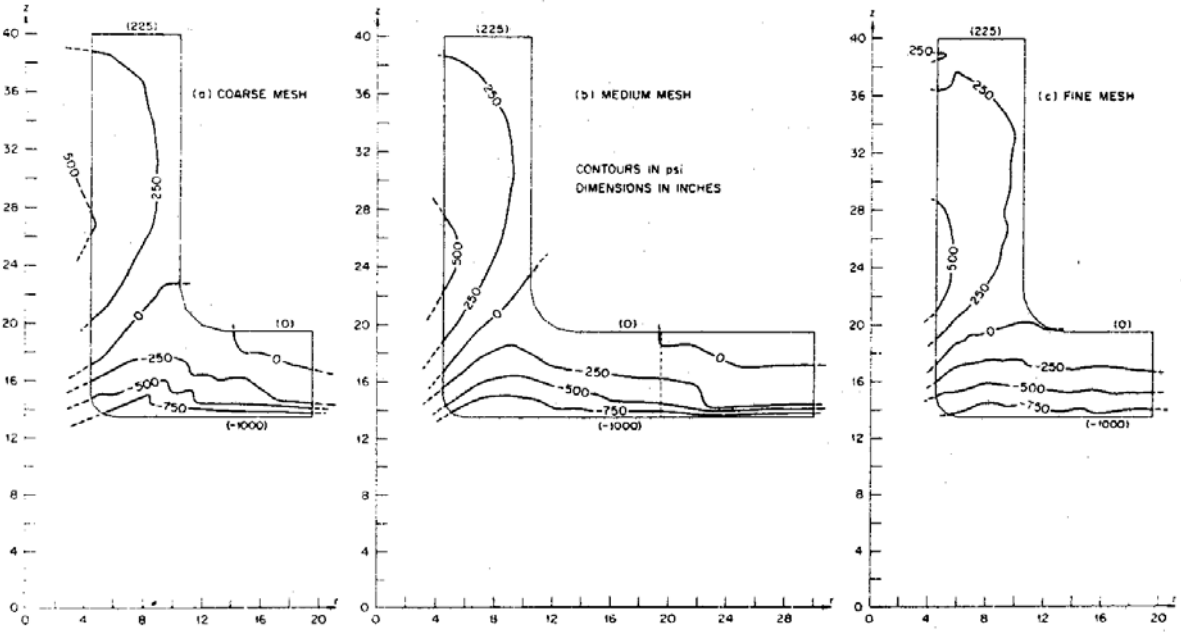

Fig. 11. Axial Stress (σ_z) Contours on Longitudinal Section.

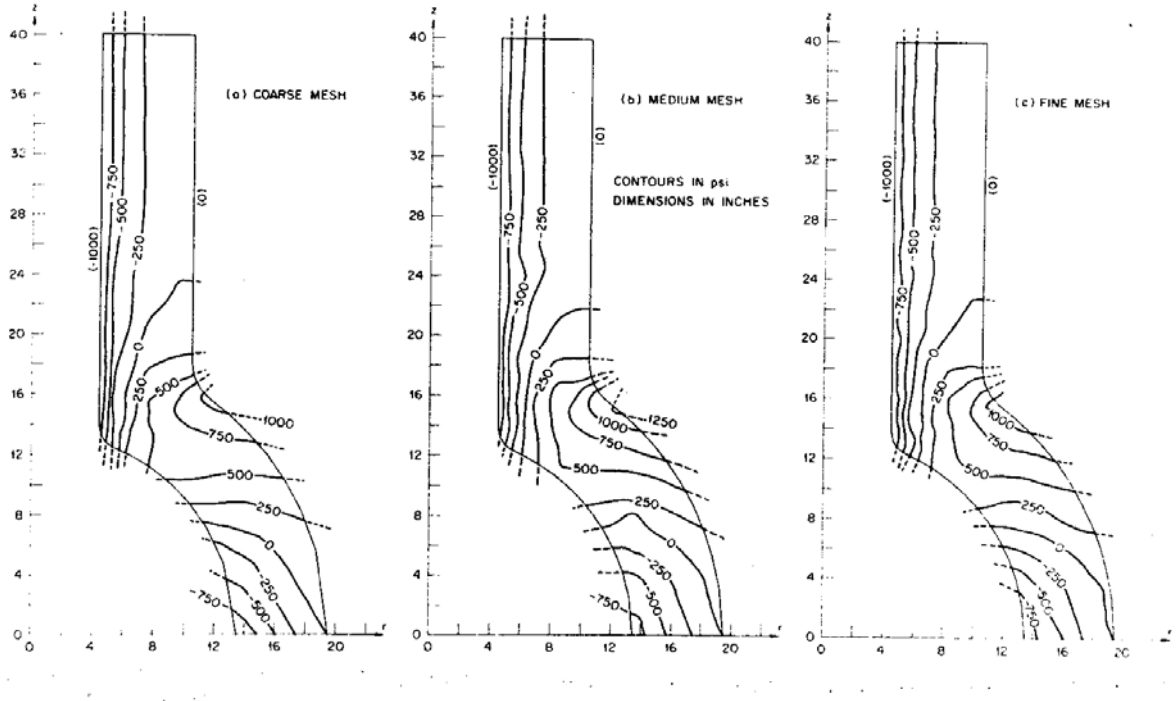

Fig. 12. Radial Stress (σ_r) Contours on Transverse Section.

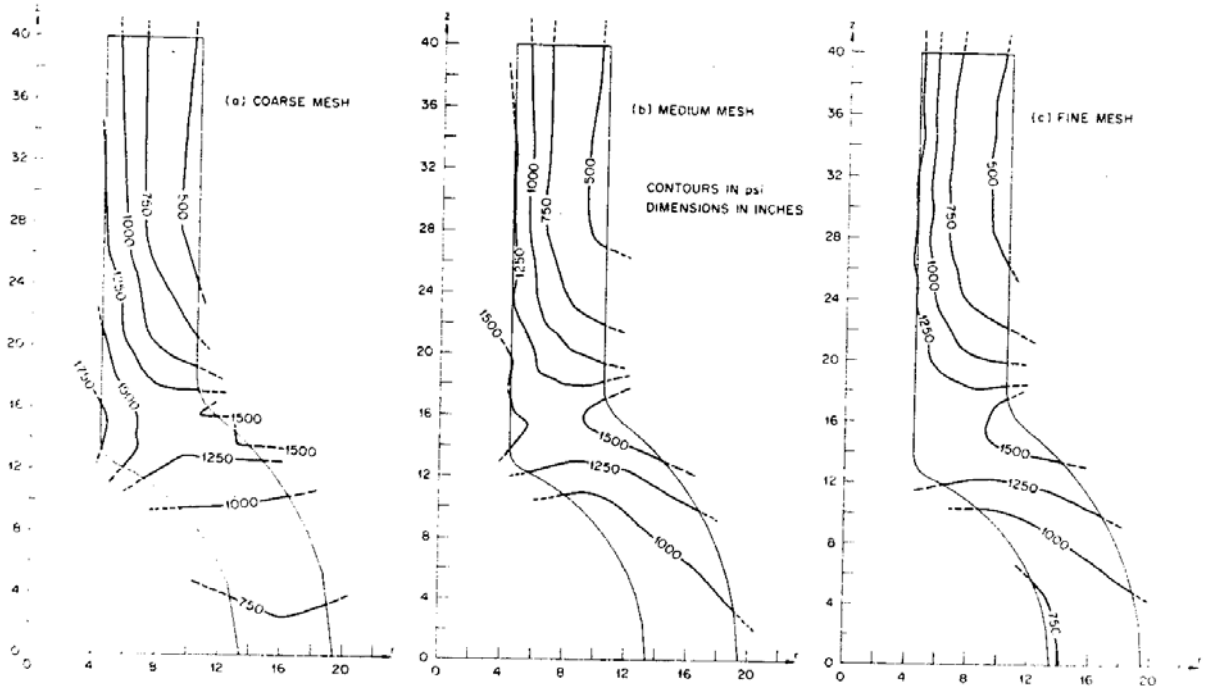

Fig. 13. Circumferential Stress (σ_θ) Contours on Transverse Section.

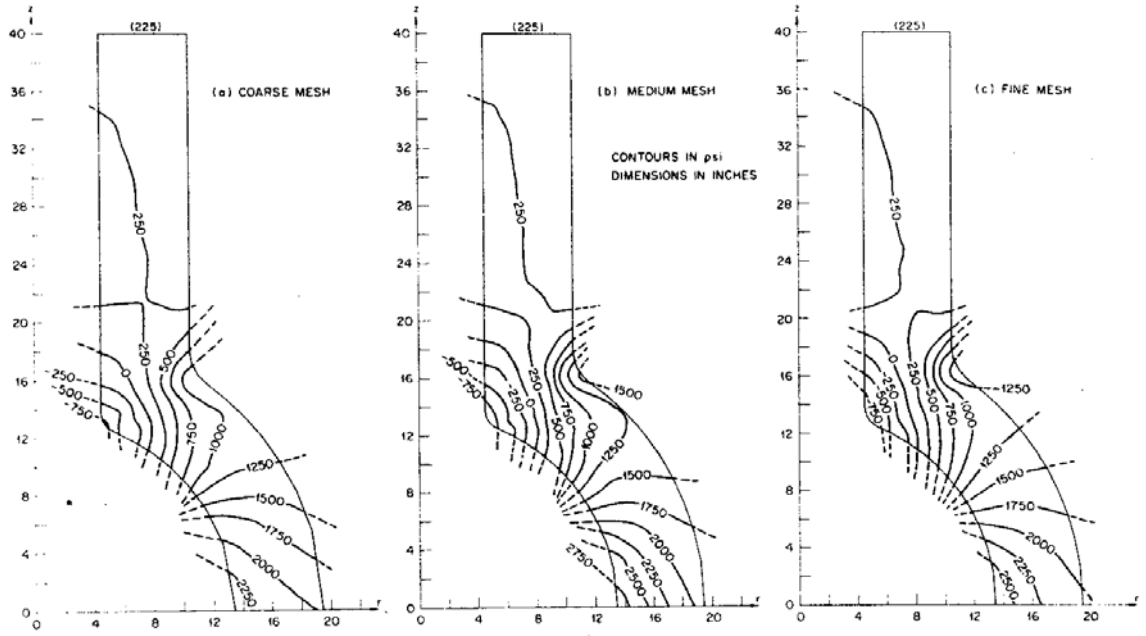

Fig. 14. Axial Stress (σ_z) Contours on Transverse Section.

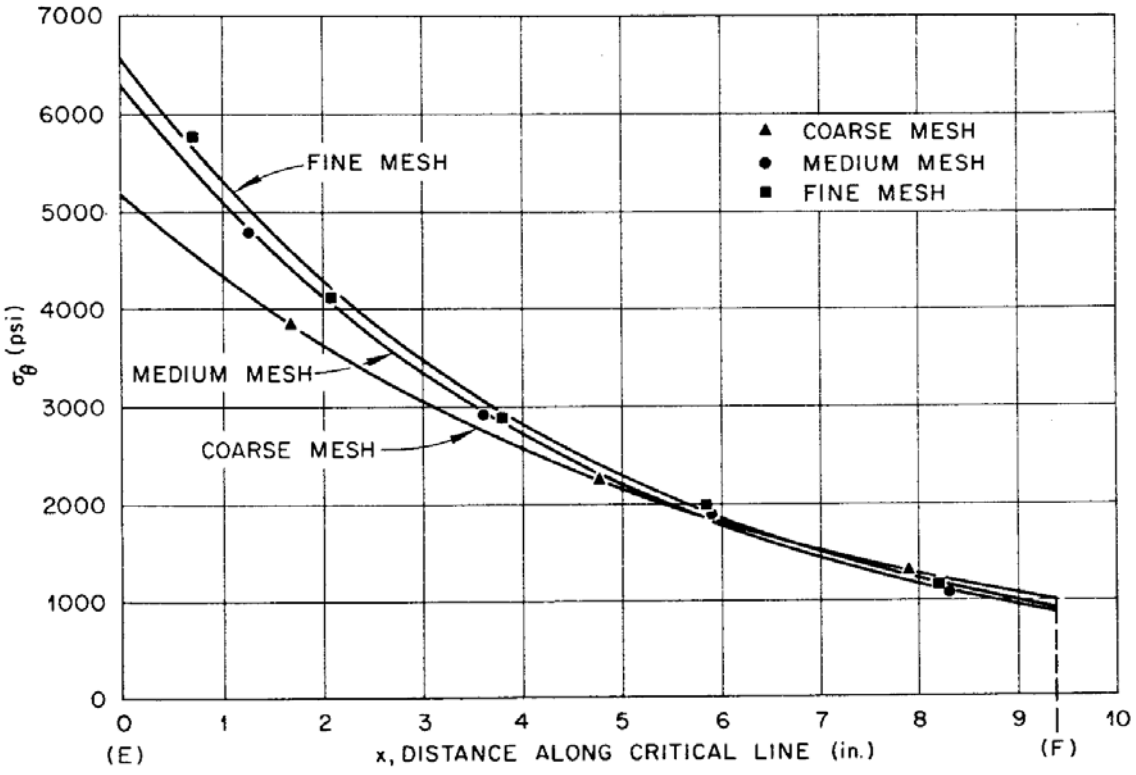

Fig. 15. Circumferential Stress Extrapolation to the Surface, along Critical Line.

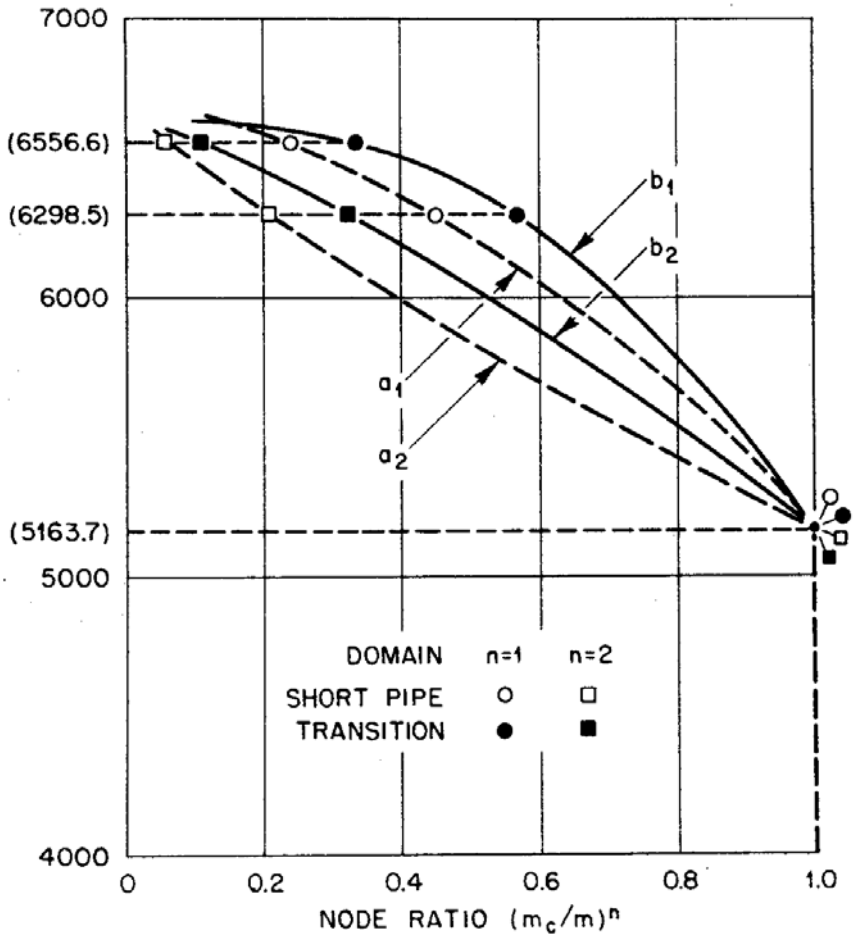

Fig. 16. Extrapolation of Maximum Stress in the Continuum.